Nanoscale

PAPER

View Article Online
View Journal | View Issue

Cite this: *Nanoscale*, 2014, **6**, 10134

Protection of centre spin coherence by dynamic nuclear spin polarization in diamond

Gang-Qin Liu,†[a] Qian-Qing Jiang,†[a] Yan-Chun Chang,[a] Dong-Qi Liu,[a] Wu-Xia Li,[a] Chang-Zhi Gu,[ab] Hoi Chun Po,[c] Wen-Xian Zhang,[d] Nan Zhao[e] and Xin-Yu Pan*[ab]

Received 14th April 2014
Accepted 6th June 2014

DOI: 10.1039/c4nr02007c

www.rsc.org/nanoscale

We experimentally investigate the protection of electron spin coherence of a nitrogen-vacancy (NV) centre in diamond by dynamic nuclear spin polarization (DNP). The electron spin decoherence of an NV centre is caused by the magnetic field fluctuation of the ^{13}C nuclear spin bath, which contributes large thermal fluctuation to the centre electron spin when it is in an equilibrium state at room temperature. To address this issue, we continuously transfer the angular momentum from electron spin to nuclear spins, and pump the nuclear spin bath to a polarized state under the Hartmann–Hahn condition. The bath polarization effect is verified by the observation of prolongation of the electron spin coherence time (T_2^*). Optimal conditions for the DNP process, including the pumping pulse duration and repeat numbers, are proposed by numerical simulation and confirmed by experiment. We also studied the depolarization effect of laser pulses. Our results provide a new route for quantum information processing and quantum simulation using the polarized nuclear spin bath.

1 Introduction

The nitrogen-vacancy (NV) centre in diamond is an attractive system to implement quantum computing,[1–9] nano-magnetometry[10–17] and nano-thermometry.[18,19] These applications rely heavily on the centre spin coherence. In general, the thermal fluctuations of the unpolarized spin bath cause fast decoherence of the centre spin,[20–25] thus polarizing the nuclear spin bath and suppressing their inhomogeneous broadening, which will prolong centre spin coherence time, can benefit all these applications.

Unfortunately, establishing significant nuclear spin polarization in thermal equilibrium is usually difficult, because of the small nuclear spin Zeeman energy ω_{zeeman} compared with the thermal energy k_BT (*i.e.* $\omega_{zeeman} \ll k_BT$). Several strategies have been demonstrated to build nuclear spin polarization in NV systems. One strategy is mapping the optically polarized electron spin state to nearby nuclear spins.[4,9,26] In this scheme, only a small number of nuclear spins, with known hyperfine interactions, are polarized by state-selective manipulation of the centre electron spin. However, the other weak coupled nuclear spins, with unknown hyperfine interactions, are the dominant sources of center spin decoherence and cannot be polarized by this scheme. Another strategy is using excited state level anti-crossing (ESLAC) to build a polarization transfer channel, and polarize both centre electron spin and nearby nuclear spins by a short laser pulse.[27–31] This easy and fast method can polarize nuclear spins with high fidelity, but the polarization mechanism also limits its applications. The laser pulse, which is necessary to readout electron spin state, will completely destroy the nuclear spin state under ESLAC.

Here we demonstrate a controllable scheme, named dynamic nuclear spin polarization (DNP),[32–34] to build simultaneous polarization of those weakly coupled nuclear spins, even with unknown hyperfine interactions. We employ the Hartmann–Hahn (HH) condition[35] to build a polarization passage between centre electron spin and the bath spins, and transfer the polarization from the electron spin to the nuclear spins. This strategy has been implemented in the NV system under a strong magnetic field (>5000 Gauss),[36] as the reversal effect of nuclear spin polarization is almost suppressed. Our results suggest that a much smaller magnetic field (650 Gauss) is also able to build the bath spin polarization, and the laser pulse plays an important role in the limitation of the polarization effect. The optimal conditions for building the polarization transfer channel are found by numerical simulation and confirmed by experiment.

2 Polarization transfer channel

A home-built confocal microscope system with microwave (MW) components is used to initialize, manipulate and readout the

[a]*Beijing National Laboratory for Condensed Matter Physics, Institute of Physics, Chinese Academy of Sciences, Beijing 100190, China. E-mail: xypan@aphy.iphy.ac.cn; Fax: +86 10 8264 0266; Tel: +86 10 8264 9211*
[b]*Collaborative Innovation Center of Quantum Matter, Beijing 100871, China*
[c]*Department of Physics, The Chinese University of Hong Kong, Shatin, New Territories, Hong Kong, China*
[d]*School of Physics and Technology, Wuhan University, Wuhan, Hubei 430072, China*
[e]*Beijing Computational Science Research Center, Beijing 100084, China*
† These authors contributed equally to this work.

spin state of single NV centres in pure diamond (with nitrogen concentration ≪5 ppb). To enhance the photon collection efficiency, a 12 μm diameter solid immersion lens (SIL) is etched above a selected NV centre.[37] The microwave pulses, which are used to manipulate electron spin states, are delivered to the NV centres through a coplanar waveguide (CPW) antenna deposited close to the SIL. A permanent magnet is used to generate the external magnetic field (500–660 Gauss) along the [111] direction of the crystal. On the one hand, the magnetic field lifts the degeneracy of the $m_s = \pm 1$ states of the electron spin; on the other hand, the host ^{14}N nuclear spin is also polarized to the $m_I = +1$ sublevel by ESLAC[27–31] under such magnetic field. All these experiments are done at room temperature.

2.1 Hartmann–Hahn condition

The Hamiltonian of a negatively charged NV centre (NV^-) in pure diamond under an external magnetic field $\mathbf{B}$ is:[22,24]

$$H = \Delta S_z^2 - \gamma_e \mathbf{B}\cdot\mathbf{S} - \gamma_c \mathbf{B}\cdot\sum_i \mathbf{I}_i + S_z \sum_i \mathbf{A}_i\cdot\mathbf{I}_i \qquad (1)$$

where $\mathbf{S}$ is the NV spin operator, and $\mathbf{I}$ represents the nuclear spin operator. $\Delta = 2.87$ GHz is the zero-field splitting of the spin-1 ground states. $\gamma_e = -1.76 \times 10^{11}$ T^{-1} s^{-1} and $\gamma_c = 6.73 \times 10^7$ T^{-1} s^{-1} are the gyromagnetic ratios of electron spins and ^{13}C nuclear spins. $\mathbf{A}_i$ is the hyperfine tensor for $\mathbf{I}_i$. The hyperfine interaction with surrounding ^{13}C nuclear spins causes decoherence of centre spins. In general conditions, the spin bath is in thermal equilibrium, and the thermal fluctuation of the unpolarized nuclear spin bath leads to fast decoherence of centre spin[20–24] [Fig. 1(a)]. In contrast, if one prepares the nuclear spin bath to a polarized state, the centre spin coherence can be well protected and an enhancement of coherence time is expected [Fig. 1(b)].[34]

An efficient polarization transfer channel is built up by driving the electron spin with the Hartmann–Hahn condition,[35] where the nuclear spins are resonant with the electron spin in the rotating frame [Fig. 1(c)]. Generally speaking, for two spins with different precession frequencies, the angular momentum transfer process is inefficient due to the energy mismatch. In order to overcome the energy mismatch, one can drive the spins, and adjust the driving power (or Rabi frequency), so that they are in resonance in the rotating frame.[38–40] In our experiment, we drive the electron spin with microwave pulses, and tune the Rabi frequency (Ω_R) of electron spin so that the Hartmann–Hahn condition $\Omega_R = \gamma_c \mathbf{B}$ is satisfied. In this case, the Rabi frequency is in resonance with the Larmor frequency of the ^{13}C bath spins under a certain external magnetic field [see the inset figure of Fig. 1(c)]. Physically, the energy mismatch is compensated by the microwave driving power, and the angular momentum transfer process can occur efficiently.

2.2 Polarization transfer channel

To demonstrate the controllable transfer of spin polarization, we change the power of the microwave pulse, and measure the decay behavior of the electron spin Rabi oscillation. Fig. 2 shows that the amplitude decay rate of the Rabi oscillation strongly depends on the microwave power. In particular, when the Hartmann–Hahn condition is fulfilled, the amplitude decay rate of the Rabi oscillation is drastically increased. While in the off-resonant regions, either $\Omega_R \gg \gamma_c \mathbf{B}$ or $\Omega_R \ll \gamma_c \mathbf{B}$, the Rabi oscillation amplitude decays at a much slower rate, indicating that the polarized centre spin is well isolated from the surrounding bath spins. We fit the Rabi oscillation envelope, and extract the characteristic decay time $T_{1\rho}$. The dependence of decay time $T_{1\rho}$ on Rabi frequency Ω_R is summarized in Fig. 2(d). The decrease of $T_{1\rho}$ under the Hartmann–Hahn condition is

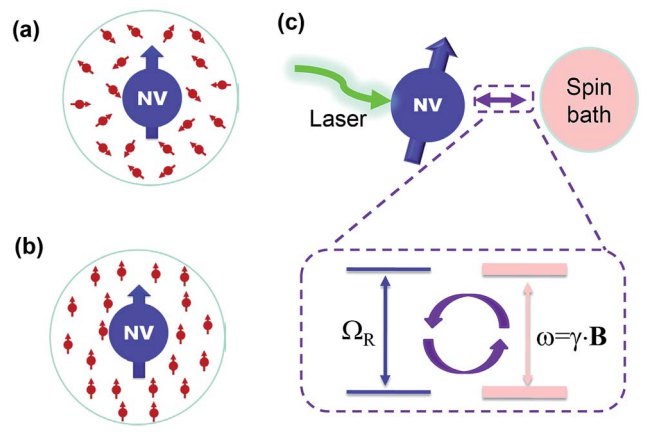

Fig. 1 General schematic. (a) Spin bath in thermal equilibrium, red arrows represent ^{13}C nuclear spins around centre electron spins. The thermal fluctuations of the unpolarized spin bath usually cause fast decoherence of the centre spin. (b) After DNP, the ^{13}C nuclear spins close to the NV centre are polarized, and centre spin coherence can be well protected by the polarized bath. (c) Polarization transformation around an NV centre in diamond. Inset, the Hartmann–Hahn condition.

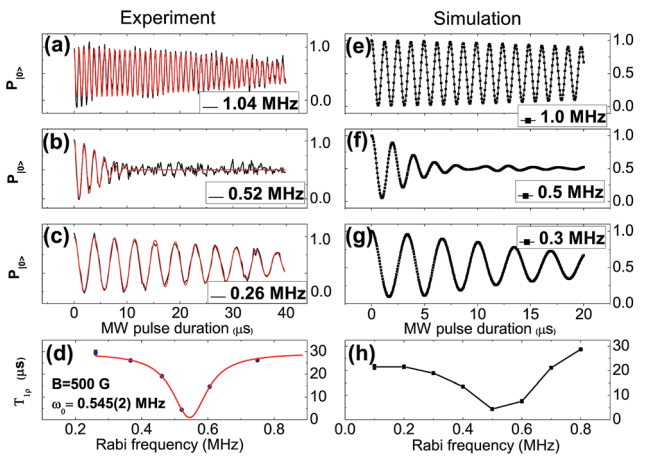

Fig. 2 Hartmann–Hahn resonance between electron spin and nearby ^{13}C nuclear spins. (a–c) Rabi oscillation of centre electron spin driven by different MW power under $\mathbf{B} = 500$ Gauss. (d) Dependence of the envelope decay time ($T_{1\rho}$ time) on the Rabi frequency. A dramatic decay was observed at the Hartmann–Hahn condition ($\Omega_R = \gamma_c \mathbf{B} = 545$ kHz), which indicates that the spin polarization transfer channel was built under such condition. (e–h) Numerical simulation results of (a–d).

caused by the resonant flip-flop process between nuclear bath spins and the electron spin in the rotating frame. While outside the resonant regime, the direct flip-flop process is suppressed, and only the much weaker second-order processes contribute to decay of the Rabi oscillation amplitude.[41]

We use numerical simulation to confirm the physical picture of this resonant decay of Rabi oscillation.[24] Nuclear spin baths according to the ^{13}C natural abundance (1.1%) are randomly generated, and the one providing similar coherence time to the measured value is chosen. We then calculate the coherent evolution of the NV center electron spin together with the first 8 nuclear spins around the center spin under MW driving. Fig. 2(e–h) show numerical simulation of the controllable Rabi decay, which indicates that the polarization transfer process can be well described by considering the hyperfine interaction between centre spins and bath spins.

3 DNP results and discussion

3.1 Pulse sequence and bath spin polarization

Fig. 3(a) shows the pulse sequence to carry out the DNP experiment. A short 532 nm laser pulse (typically 3 μs) polarizes the centre electron spin to $m_s = 0$ state with high fidelity. A $\pi/2$ MW pulse rotates the state to the x direction in the equatorial plane of its Bloch sphere. A following 90°-phase-shifted MW pulse with the same frequency locks the centre spin state along the x direction in the rotating frame for a period of time τ. The power

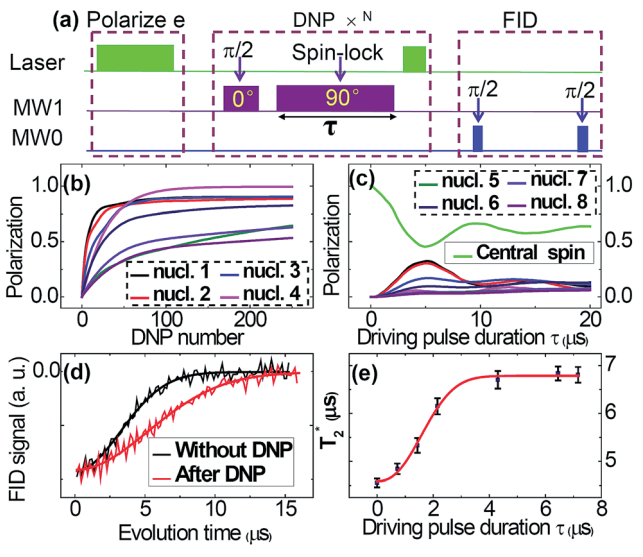

Fig. 3 Polarization transfer process and enhancement of centre spin coherence (T_2^*) time. (a) The pulse sequence used to generate (the DNP sequence) and to examine (the FID sequence) nuclear spin bath polarization. (b and c) Numerical simulations of the polarization transfer process. For 8 random located ^{13}C nuclear spins around an NV centre, the dependence of spin polarization on (b) DNP number and (c) spin-lock driving duration are monitored. (d) Experimental measured FID signals without (black line) and after (red line) DNP, the prolongation of the dephasing time (from 4.6 μs to 7.4 μs) indicates that the bath spin is polarized during the DNP process. (e) Dependence of the T_2^* time on the DNP pumping duration, with $N = 10$. The magnetic field is 660 Gauss for these measurements.

of the spin-lock pulse is adjusted to match the HH condition, thus the optical pumped high polarization of centre spin will transfer during the spin-lock pulse. After that, another laser pulse is used to repolarize the centre spin. These polarization injection and transfer processes are repeated N times, so that a significant nuclear spin polarization is built up in the bath. Finally, we check the polarization effect by measuring the Ramsey interference.

As the polarization of the centre electron spin is leaking under the Hartmann–Hahn condition [Fig. 2(b)], its surrounding nuclear spins are expected to be polarized. Fig. 3(b) shows theoretical simulations of the bath polarizing effect. The polarizations of 8 nearest neighboring ^{13}C nuclear spins to the NV centre in a randomly generated bath configuration are presented as functions of the number N of DNP pumping cycles. To simulate the laser initialization of electron spin, for each laser pulse, we trace out the electron spin degree of freedom, and feed the resultant nuclear spin reduced density matrix as the initial bath state in the subsequent coherent evolution. The coherent evolution during the spin-locking period is calculated using the same method as that in Fig. 2. We find that about 100 cycles DNP process is enough to reach the saturated polarization for most of the nuclear spins.

Fig. 3(c) shows the dependence of polarization on spin-lock duration. The oscillation behavior demonstrates that the net polarization is transferred back and forth between the NV centre electron spin and the ^{13}C bath spins,[36] and the different oscillation frequency among the 8 nuclear spins indicates that the polarization transfer speed is strongly dependent on the hyperfine tensors. Considering the inhomogeneity of the hyperfine coupling strength and the wide distribution of transfer rate among nuclear spins, the best strategy to achieve a directional polarization transfer from electron spin to bath spins is to keep the spin-lock duration in one cycle short (*e.g.* 2 μs), and repeat the short DNP pumping process to create significant bath polarization.

3.2 Enhancement of centre spin coherence time

Fig. 3(d) shows the experimental observed enhancement of T_2^* time after DNP. In an external magnetic field of 660 Gauss, with $N = 10$ DNP pumping pulses ($\tau = 4$ μs) inserted before the Ramsey measurement sequence, the electron spin coherence shows a Gaussian shape decay with a characteristic decay time $T_2^* = 7.4(7)$ μs (red line). In comparison, the Ramsey signal without DNP, under the same magnetic field, decays faster with $T_2^* = 4.46(6)$ μs (black line). The enhancement of the T_2^* time implies the creation of the bath polarization and the suppression of thermal fluctuations by DNP pumping. We note that ESLAC may also contribute to the nuclear spin polarization. Under a small magnetic field of about 100 Gauss, this centre has a typical decoherence time of $T_2^* = 1.6(1)$ μs [see data in ref. 26], which is much shorter than $T_2^* = 4.46(6)$ μs under $B = 660$ Gauss. This enhancement is partly caused by the polarization of strongly coupled nuclear spins under ESLAC,[27–31] and partly caused by the "freeze effect" of the large magnetic field.[25] However, the difference of T_2^* with and without DNP under the

same magnetic field, is mainly caused by the polarization transfer under the HH condition, this is further confirmed by the spin-lock duration and laser-power dependence of the DNP effect, as we show below.

Fig. 3(e) presents the dependence of electron spin decoherence time on the spin-lock duration τ. We find a typical 2 μs lock time is sufficient to transfer the centre spin polarization, and a longer lock time has little improvement, which is consistent with the polarization oscillation period shown in numerical simulation results [Fig. 3(c)]. The saturated value of T_2^* is increased by a factor of 2 in comparison with the case without DNP pumping. However, this enhancement ratio is much less than that if all the surrounding ^{13}C nuclear spins in the bath would be highly polarized. The reason for the limitation of the dephasing time is the possible depolarizing dynamics of the bath spins, including the influence of the laser pulse and the fluctuation of the external magnetic field.

3.3 Influence of the laser power

To understand the depolarization effect in the DNP process, we investigate the influence of laser power on the DNP effect (Fig. 4). Firstly, the laser pulses with power ranging from 50 μW to 1.3 mW were used to carry out the same measurement sequence shown in Fig. 3(a). The optical readout time for electron spin states is also adjusted to ensure high readout fidelity in different laser powers. For a fair comparison, free induction decays under the same conditions are also measured and plotted (black scatters). As depicted in Fig. 4(b), the enhancement of electron spin dephasing time are observed for all the 4 measured cases (red scatters), and lower laser power gives longer decoherence time. Fig. 4(c) shows the longest coherence time we observed for this NV under the same magnetic field after optimizing the laser power (50 μW was used). The observed $T_2^* = 8.0(2)$ μs is nearly two times comparing with the dephasing time without DNP.

To further characterize the influence of the laser pulse, we insert an extra laser pulse (100 μs) between the DNP and the standard FID probe pulse [see Fig. 4(a) for pulse sequence]. The measured result is presented by Fig. 4(d), the resultant dephasing time $T_2^* = 4.9(2)$ μs is just a little longer than the dephasing time without DNP pulses [Fig. 3(d), black line], indicating the nuclear spin bath polarization built by the DNP process is significantly destroyed by the laser pulse. A comparison pulse sequence with the laser pulse replaced by a free waiting segment [Fig. 4(a), 100 μs] gives a longer time $T_2^* = 5.4(2)$ μs [see Fig. 4(e)] than the case shown in Fig. 4(d), but not as long as the normal DNP without inserting segment. This can be understood by considering the repetitive measurement process. Since the nuclear bath spins evolve in a time scale of hundreds of microseconds, and the FID probe sequence takes only several microseconds, the adjacent DNP interact with each other in repetitive measurement, thus the effective number N' for the continuous measurement is larger than N. When the 100 μs waiting pulse is inserted between the DNP and FID sequence, the overlapped influence of adjacent DNP sequences become weaker, and the effective number N' decrease, thus the electron spin dephasing time is shorter than that obtained with continuous measurement.

We attribute the laser induced depolarization effect to the different hyperfine interactions with electron spin in the ground state or excited state.[6] Under laser excitation, the electron will be elevated to the excited state and decay back to the ground state randomly with rates determined by the laser power and the lifetime of the excited state. Seen by surrounding ^{13}C nuclear spins, the transition of electron state induces a randomly changing hyperfine field, which causes the nuclear spin flipping. In other words, the excitation of an electron will limit the T_1 time of the surrounding ^{13}C nuclear spins, resulting in the depolarization effect. This laser induced depolarization effect can be suppressed by carefully tuning the magnetic field direction (along the [111] of diamond crystal), and increasing the magnetic field strength to prolong the T_1 time of nuclear spins.[6,36,42]

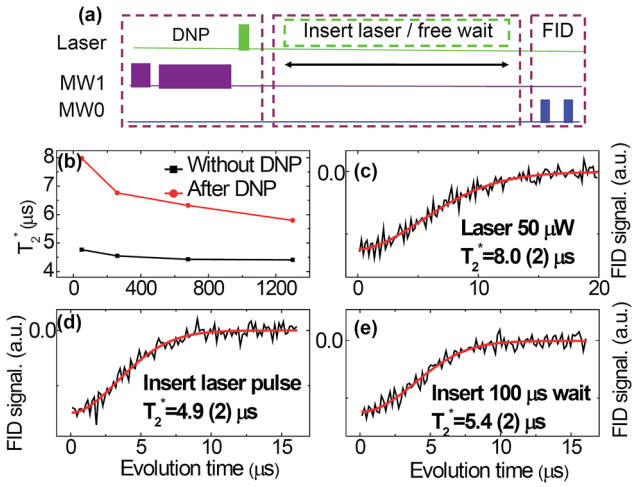

Fig. 4 Influence of laser pulse. (a) Pulse sequence used to investigate laser depolarizing effect. (b) Laser power dependence. The red (black) scatters are the measured T_2^* times after (without) DNP pumping process under 4 different laser powers. Lower laser power gives stronger enhancement of centre spin coherence time. (c) The FID result with DNP pumping at the optimized laser power (50 μW). The T_2^* time of electron spin is ~2 times longer than the case without DNP pumping. (d) FID after adding depolarizing laser pulse. The insertion of laser pulses will depolarize the bath spin polarization built by the DNP process, resulting in a dephasing time close to the case without DNP. (d) FID after adding free waiting segment. The extra waiting time decreases the effective number of DNP cycles, so an in-between dephasing time is observed.

3.4 Discussion

A controllable nuclear spin polarization scheme is particularly useful for quantum computing and quantum simulation[43] applications. Comparing with another widely used coherence protection technique, dynamical decoupling (DD),[44–47] which can average out bath spin fluctuation by flipping the centre spin state, DNP is an active strategy to suppress the thermal fluctuations. The polarization of the nuclear spins can persist for hundreds of microseconds, during which many manipulations can be applied to the centre electron spin. In this sense, DNP is compatible with quantum gate operations, while the coherence

protection effect of a traditional DD sequence is limited in between the pulses, and hard to be integrated with the quantum gate.[9,26,48]

The enhanced T_2^* time has immediate application in the sensing of DC magnetic fields.[12] Magnetic sensitivity is proportional to $\frac{1}{\sqrt{T_2^*}}$, thus an enhancement of 2 times of T_2^* corresponds to a $\frac{1}{\sqrt{2}}$ improvement in sensitivity. But this comes at a price of extra time consumption in polarizing the nuclear spin bath, which removes the advantage of T_2^* enhancement. However, a NV center under the HH condition can be utilized as a sensitive and robust probe to detect AC magnetic signals. As demonstrated in ref. 36, 49 and 50, one can adjust the Rabi frequency of a NV electron spin to match the Larmor frequency of target spins, thus selectively amplifying the magnetic signal of target spins, while keeping other background magnetic noise well decoupled.

Another merit of this scheme is it works for all the weakly coupled[13] nuclear spins. Considering ^{12}C isotopically enriched diamond,[6] with much weaker dipole–dipole coupling strength in the purified bath, the requirement of suppressing the non-secular (energy non-conserving) spin flipping will be more easily fulfilled in a weaker magnetic field, and the optimal spin-lock duration is expected to be longer than the natural abundance sample, since the polarization transfer speeds of these weakly coupled nuclear spins are much slower.

Our results also open a new way to investigate the nuclear spin diffusion in a NV system. The quantum evolution of the nuclear bath spins causes centre spin decoherence in a time scale of T_2,[22,24] which is a crucial time for quantum information processing and quantum metrology applications. Ideally, if the bath is prepared in a fully polarized state (all ^{13}C nuclear spins pointing along the same direction), the flip-flop process will be greatly suppressed. In this case, the T_2 time should be also improved a lot. In our experiment, the bath spin polarization is far from the ideal case, and no obvious enhancement of T_2 is observed.

4 Conclusion

In summary, we observed the polarization transfer between centre electron spin and ^{13}C nuclear bath spins under the Hartmann–Hahn condition, and investigated the ^{13}C nuclear spin dynamic polarization effect. About 2 times longer centre spin dephasing time has been observed. The polarization of the spin bath can be built in several microseconds in continuous measurement and persist for hundreds of microseconds. We found that the pumping laser pulse also plays an important role in the depolarization effect. These findings potentially open a new way to investigate the dynamics of spin baths, which is a key issue in quantum computing and quantum simulation, sensitive nano-magnetometry and nano-thermometry.

Acknowledgements

We thank Fedor Jelezko for the helpful discussion. This work was supported by National Basic Research Program of China (973 Program project and Nos. 2014CB921402 and 2009CB930502), the Strategic Priority Research Program of the Chinese Academy of Sciences (nos XDB07010300), and the National Natural Science Foundation of China (Grants nos 10974251, 91123004, 11104334, 51272278 and 11275139). N.Z. acknowledges NKBRP (973 Program) 2014CB848700, and NSFC no. 11374032.

References

1 F. Jelezko, T. Gaebel, I. Popa, M. Domhan, A. Gruber and J. Wrachtrup, *Phys. Rev. Lett.*, 2004, **93**, 130501.
2 J. Wrachtrup and F. Jelezko, *J. Phys.: Condens. Matter*, 2006, **18**, S807.
3 L. Childress, M. G. Dutt, J. Taylor, A. Zibrov, F. Jelezko, J. Wrachtrup, P. Hemmer and M. Lukin, *Science*, 2006, **314**, 281–285.
4 M. G. Dutt, L. Childress, L. Jiang, E. Togan, J. Maze, F. Jelezko, A. Zibrov, P. Hemmer and M. Lukin, *Science*, 2007, **316**, 1312–1316.
5 T. D. Ladd, F. Jelezko, R. Laflamme, Y. Nakamura, C. Monroe and J. L. O'Brien, *Nature*, 2010, **464**, 45–53.
6 P. C. Maurer, G. Kucsko, C. Latta, L. Jiang, N. Y. Yao, S. D. Bennett, F. Pastawski, D. Hunger, N. Chisholm, M. Markham, *et al.*, *Science*, 2012, **336**, 1283–1286.
7 H. Bernien, B. Hensen, W. Pfaff, G. Koolstra, M. Blok, L. Robledo, T. Taminiau, M. Markham, D. Twitchen, L. Childress, *et al.*, *Nature*, 2013, **497**, 86–90.
8 G. Waldherr, Y. Wang, S. Zaiser, M. Jamali, T. Schulte-Herbrüggen, H. Abe, T. Ohshima, J. Isoya, J. Du, P. Neumann, *et al.*, *Nature*, 2014, **506**, 204.
9 T. H. Taminiau, J. Cramer, T. van der Sar, V. V. Dobrovitski and H. R. Hanson, *Nat. Nanotechnol.*, 2014, **9**, 171–176.
10 G. Balasubramanian, I. Chan, R. Kolesov, M. Al-Hmoud, J. Tisler, C. Shin, C. Kim, A. Wojcik, P. R. Hemmer, A. Krueger, *et al.*, *Nature*, 2008, **455**, 648–651.
11 J. Maze, P. Stanwix, J. Hodges, S. Hong, J. Taylor, P. Cappellaro, L. Jiang, M. G. Dutt, E. Togan, A. Zibrov, *et al.*, *Nature*, 2008, **455**, 644–647.
12 J. Taylor, P. Cappellaro, L. Childress, L. Jiang, D. Budker, P. Hemmer, A. Yacoby, R. Walsworth and M. Lukin, *Nat. Phys.*, 2008, **4**, 810–816.
13 N. Zhao, J.-L. Hu, S.-W. Ho, J. T. Wan and R. Liu, *Nat. Nanotechnol.*, 2011, **6**, 242–246.
14 N. Zhao, J. Honert, B. Schmid, M. Klas, J. Isoya, M. Markham, D. Twitchen, F. Jelezko, R.-B. Liu, H. Fedder, *et al.*, *Nat. Nanotechnol.*, 2012, **7**, 657–662.
15 T. H. Taminiau, J. J. T. Wagenaar, T. van der Sar, F. Jelezko, V. V. Dobrovitski and R. Hanson, *Phys. Rev. Lett.*, 2012, **109**, 137602.
16 S. Kolkowitz, Q. P. Unterreithmeier, S. D. Bennett and M. D. Lukin, *Phys. Rev. Lett.*, 2012, **109**, 137601.
17 F. Shi, X. Kong, P. Wang, F. Kong, N. Zhao, R.-B. Liu and J. Du, *Nat. Phys.*, 2014, **10**, 21–25.
18 D. M. Toyli, F. Charles, D. J. Christle, V. V. Dobrovitski and D. D. Awschalom, *Proc. Natl. Acad. Sci. U. S. A.*, 2013, **110**, 8417–8421.

19 P. Neumann, I. Jakobi, F. Dolde, C. Burk, R. Reuter, G. Waldherr, J. Honert, T. Wolf, A. Brunner, J. H. Shim, *et al.*, *Nano Lett.*, 2013, **13**, 2738–2742.
20 W. M. Witzel and S. Das Sarma, *Phys. Rev. B: Condens. Matter Mater. Phys.*, 2006, **74**, 035322.
21 L. Cywiński, W. M. Witzel and S. Das Sarma, *Phys. Rev. Lett.*, 2009, **102**, 057601.
22 J. R. Maze, J. M. Taylor and M. D. Lukin, *Phys. Rev. B: Condens. Matter Mater. Phys.*, 2008, **78**, 094303.
23 N. Mizuochi, P. Neumann, F. Rempp, J. Beck, V. Jacques, P. Siyushev, K. Nakamura, D. J. Twitchen, H. Watanabe, S. Yamasaki, F. Jelezko and J. Wrachtrup, *Phys. Rev. B: Condens. Matter Mater. Phys.*, 2009, **80**, 041201.
24 N. Zhao, S.-W. Ho and R.-B. Liu, *Phys. Rev. B: Condens. Matter Mater. Phys.*, 2012, **85**, 115303.
25 G.-Q. Liu, X.-Y. Pan, Z.-F. Jiang, N. Zhao and R.-B. Liu, *Sci. Rep.*, 2012, **2**, 432.
26 G.-Q. Liu, H. C. Po, J. Du, R.-B. Liu and X.-Y. Pan, *Nat. Commun.*, 2013, **4**, 2254.
27 V. Jacques, P. Neumann, J. Beck, M. Markham, D. Twitchen, J. Meijer, F. Kaiser, G. Balasubramanian, F. Jelezko and J. Wrachtrup, *Phys. Rev. Lett.*, 2009, **102**, 057403.
28 B. Smeltzer, J. McIntyre and L. Childress, *Phys. Rev. A*, 2009, **80**, 050302.
29 M. Steiner, P. Neumann, J. Beck, F. Jelezko and J. Wrachtrup, *Phys. Rev. B: Condens. Matter Mater. Phys.*, 2010, **81**, 035205.
30 B. Smeltzer, L. Childress and A. Gali, *New J. Phys.*, 2011, **13**, 025021.
31 A. Dréau, J.-R. Maze, M. Lesik, J.-F. Roch and V. Jacques, *Phys. Rev. B: Condens. Matter Mater. Phys.*, 2012, **85**, 134107.
32 D. Reilly, J. Taylor, J. Petta, C. Marcus, M. Hanson and A. Gossard, *Science*, 2008, **321**, 817–821.
33 X. Xu, W. Yao, B. Sun, D. G. Steel, A. S. Bracker, D. Gammon and L. Sham, *Nature*, 2009, **459**, 1105–1109.
34 W. Zhang, J.-L. Hu, J. Zhuang, J. Q. You and R.-B. Liu, *Phys. Rev. B: Condens. Matter Mater. Phys.*, 2010, **82**, 045314.
35 S. Hartmann and E. Hahn, *Phys. Rev.*, 1962, **128**, 2042.
36 P. London, J. Scheuer, J.-M. Cai, I. Schwarz, A. Retzker, M. B. Plenio, M. Katagiri, T. Teraji, S. Koizumi, J. Isoya, R. Fischer, L. P. McGuinness, B. Naydenov and F. Jelezko, *Phys. Rev. Lett.*, 2013, **111**, 067601.
37 L. Marseglia, J. Hadden, A. Stanley-Clarke, J. Harrison, B. Patton, Y.-L. Ho, B. Naydenov, F. Jelezko, J. Meijer, P. Dolan, *et al.*, *Appl. Phys. Lett.*, 2011, **98**, 133107.
38 R. Hanson, V. Dobrovitski, A. Feiguin, O. Gywat and D. Awschalom, *Science*, 2008, **320**, 352–355.
39 C. Belthangady, N. Bar-Gill, L. M. Pham, K. Arai, D. Le Sage, P. Cappellaro and R. L. Walsworth, *Phys. Rev. Lett.*, 2013, **110**, 157601.
40 A. Laraoui and C. A. Meriles, *ACS Nano*, 2013, **7**, 3403–3410.
41 V. V. Dobrovitski, A. E. Feiguin, R. Hanson and D. D. Awschalom, *Phys. Rev. Lett.*, 2009, **102**, 237601.
42 P. Neumann, J. Beck, M. Steiner, F. Rempp, H. Fedder, P. R. Hemmer, J. Wrachtrup and F. Jelezko, *Science*, 2010, **329**, 542–544.
43 J. Cai, A. Retzker, F. Jelezko and M. B. Plenio, *Nat. Phys.*, 2013, **9**, 168–173.
44 E. L. Hahn, *Phys. Rev.*, 1950, **80**, 580.
45 K. Khodjasteh and D. Lidar, *Phys. Rev. Lett.*, 2005, **95**, 180501.
46 G. De Lange, Z. Wang, D. Riste, V. Dobrovitski and R. Hanson, *Science*, 2010, **330**, 60–63.
47 C. A. Ryan, J. S. Hodges and D. G. Cory, *Phys. Rev. Lett.*, 2010, **105**, 200402.
48 T. Van der Sar, Z. Wang, M. Blok, H. Bernien, T. Taminiau, D. Toyli, D. Lidar, D. Awschalom, R. Hanson and V. Dobrovitski, *Nature*, 2012, **484**, 82–86.
49 M. Loretz, T. Rosskopf and C. L. Degen, *Phys. Rev. Lett.*, 2013, **110**, 017602.
50 J. Cai, F. Jelezko, M. B. Plenio and A. Retzker, *New J. Phys.*, 2013, **15**, 013020.